Color pages

Chapter 1.
J.C. van Dam, G.H. de Rooij, M. Heinen and F. Stagnitti; Figure 12

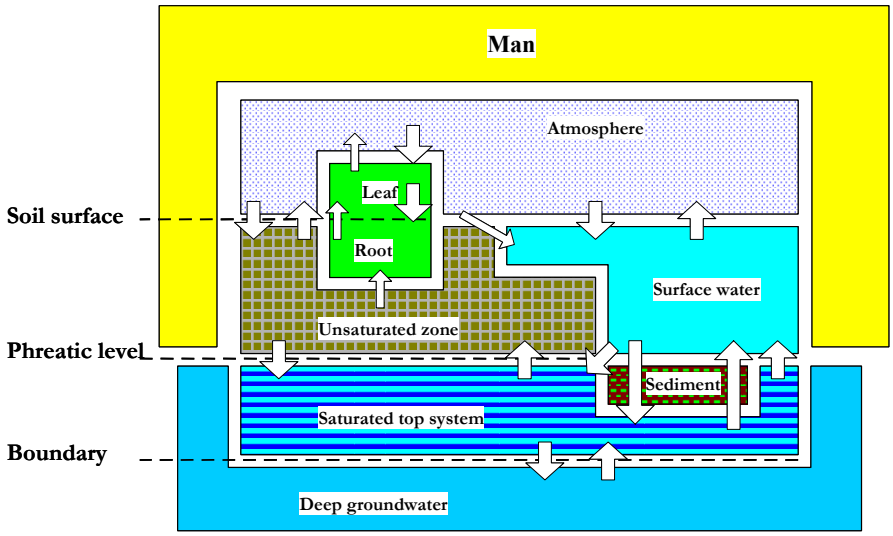

Figure 12. Subdivision of top system in separate physical domains for setup of hydrological framework (Van der Wal and Van Elswijk 2000)

Chapter 2.
M.T. van Genuchten and Jirka Šimůnek; Figures 2, 7, 8 and 9

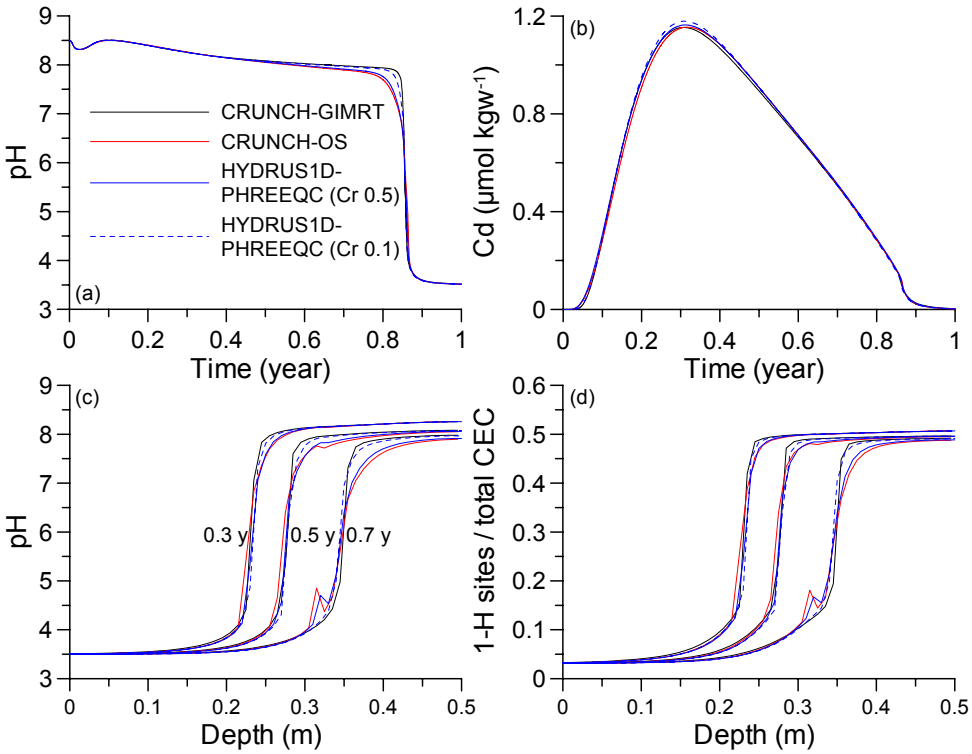

Figure 2. Selected simulation results for cation and heavy metal transport with a pH-dependent cation exchange complex: (a) and (b) pH and Cd concentration in outflow at 50 cm depth, (c) and (d) distributions versus depth of pH and fraction of deprotonated sites after 0.3, 0.5 and 0.7 y

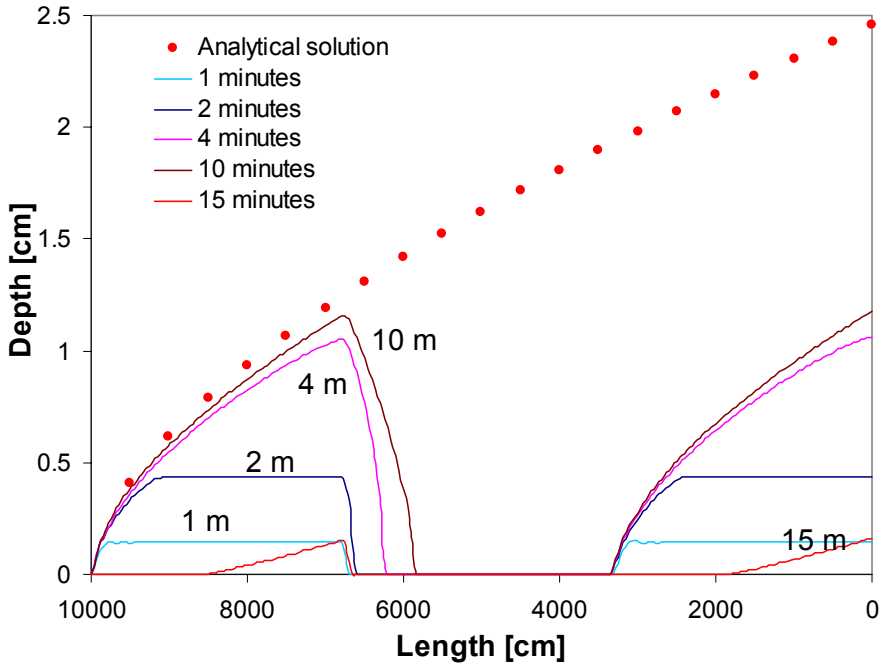

Figure 7. Depths of the water layer on the soil surface at selected times

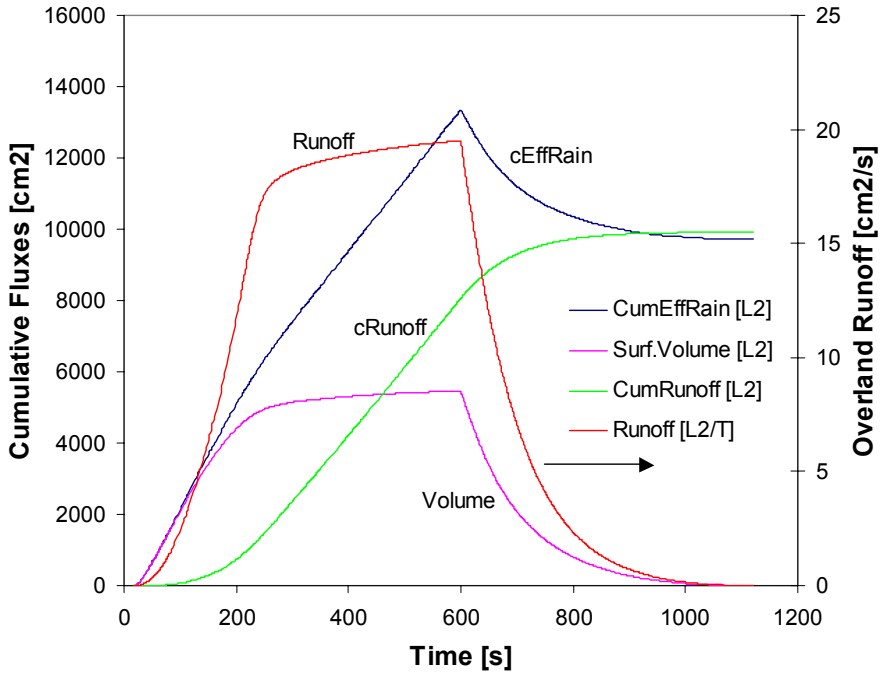

Figure 8. Actual (RunOff) and cumulative (CumRunOff) surface runoff from the hill-slope transect, the cumulative effective rainfall rate (CumEffRain), and the volume of water in the surface layer (Surf. Volume) for a 10-minute rain event

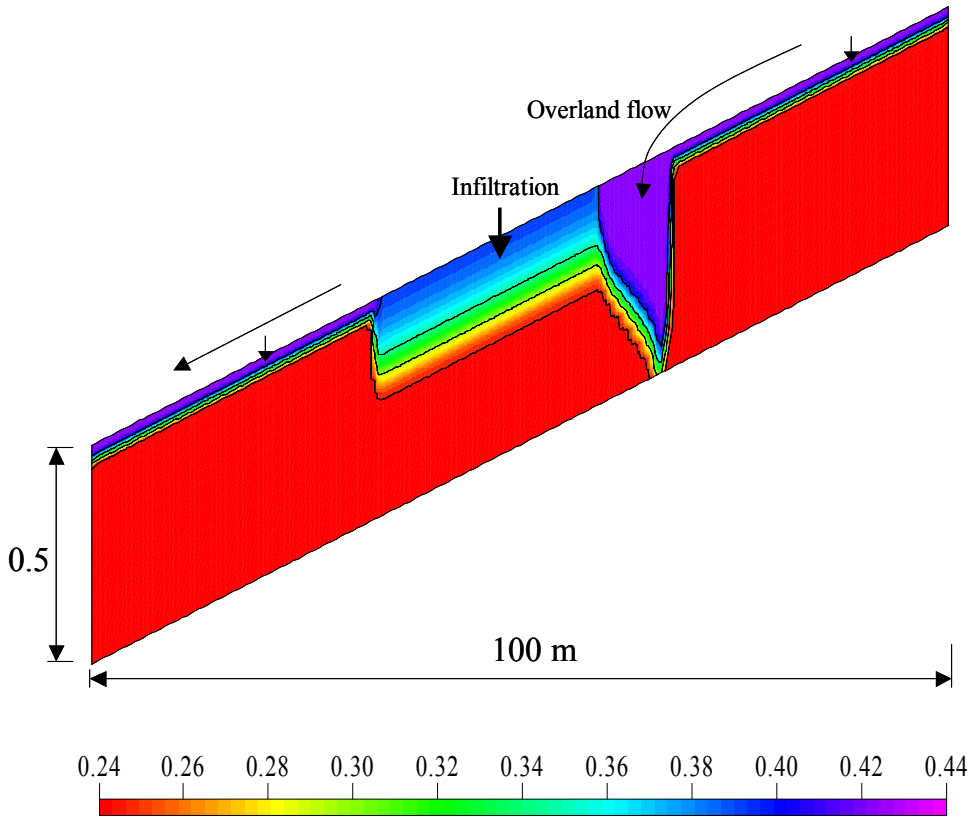

Figure 9. Contours of the water content in the soil profile 6 minutes after initiating rainfall. The soil material in the middle third of the hillside transect (between 33 and 66 m) has a 100 times higher saturated conductivity than the remaining soil

Color pages

Chapter 7.
M. Menenti, L. Jia and W.G.M. Bastiaanssen; Figure 4

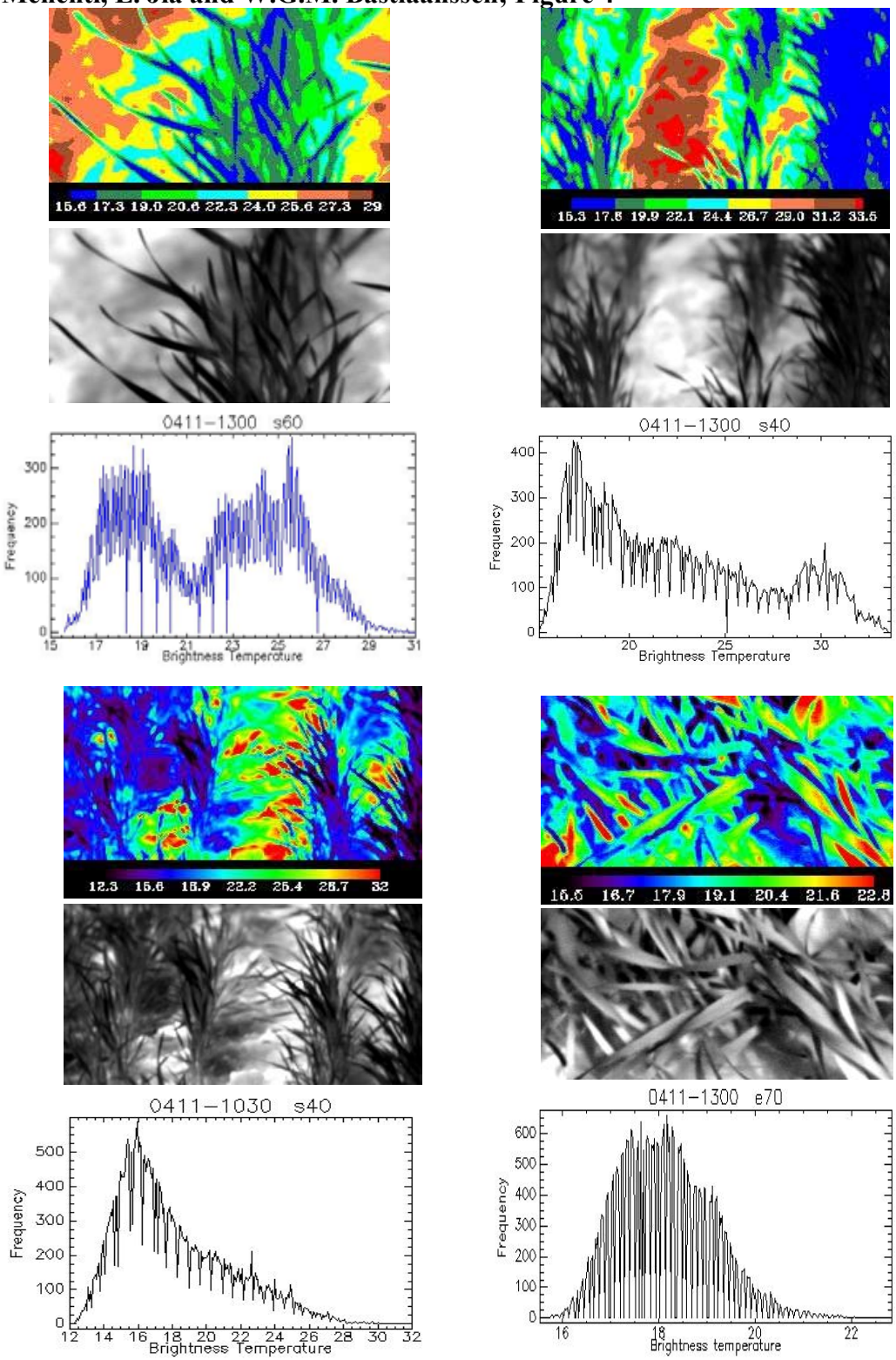

Figure 4. Top-of-canopy brightness temperature of a row crop (rows oriented S-N) measured by a thermal infrared camera at different view angles: a) from 60^0 S of target (s60), April 11, 2001 at 13.00 LST; b) from 40^0 S of target (s40), April 11, 2001 at 13.00 LST; c) from 40^0 S of target (s40), April 11, 2001 at 10.30 LST; d) from 70^0 E of target (s70), April 11, 2001 at 13.00 LST; spatial resolution changes with view angle and is 3 mm for image (c) (Jia in press)

Chapter 8.
Y.A. Pachepsky, K.R.J. Smettem, J. Vanderborght, M. Herbst, H. Vereecken, and J.H.M. Wösten; Figures 2, 3, 4, 5 and 6

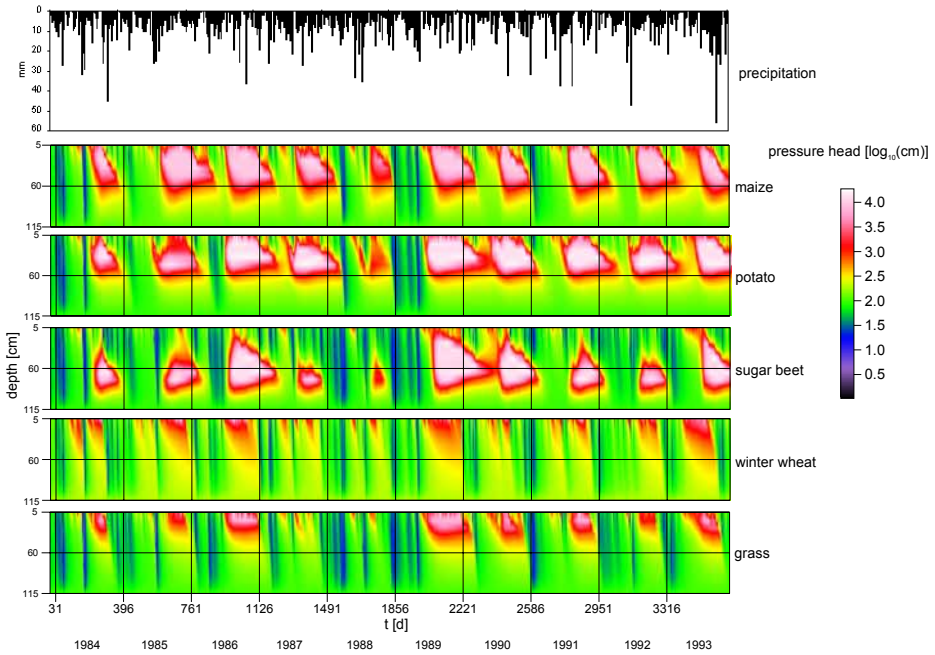

Figure 2. Effect of the crop type on the dynamic of soil matric potentials. Matric potentials are simulated by the coupled TRACE/SUCROS model

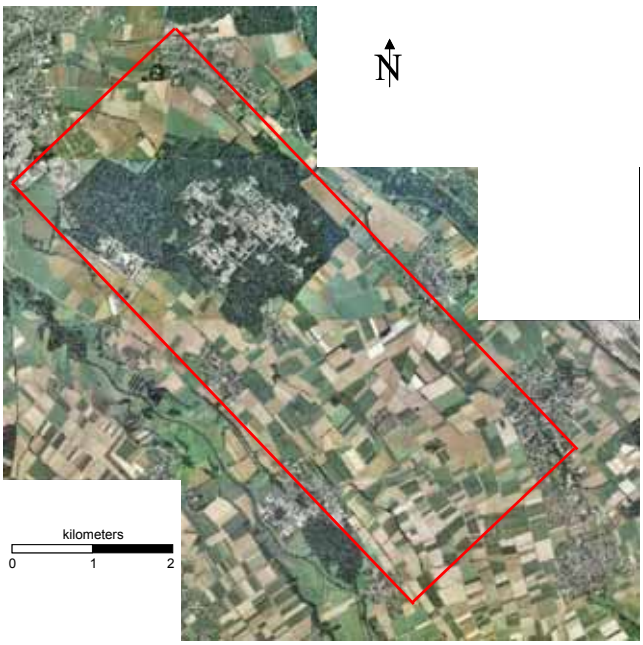

Figure 3. Areal view of the PEGASE test-site ‘Zwischenscholle’

Color pages

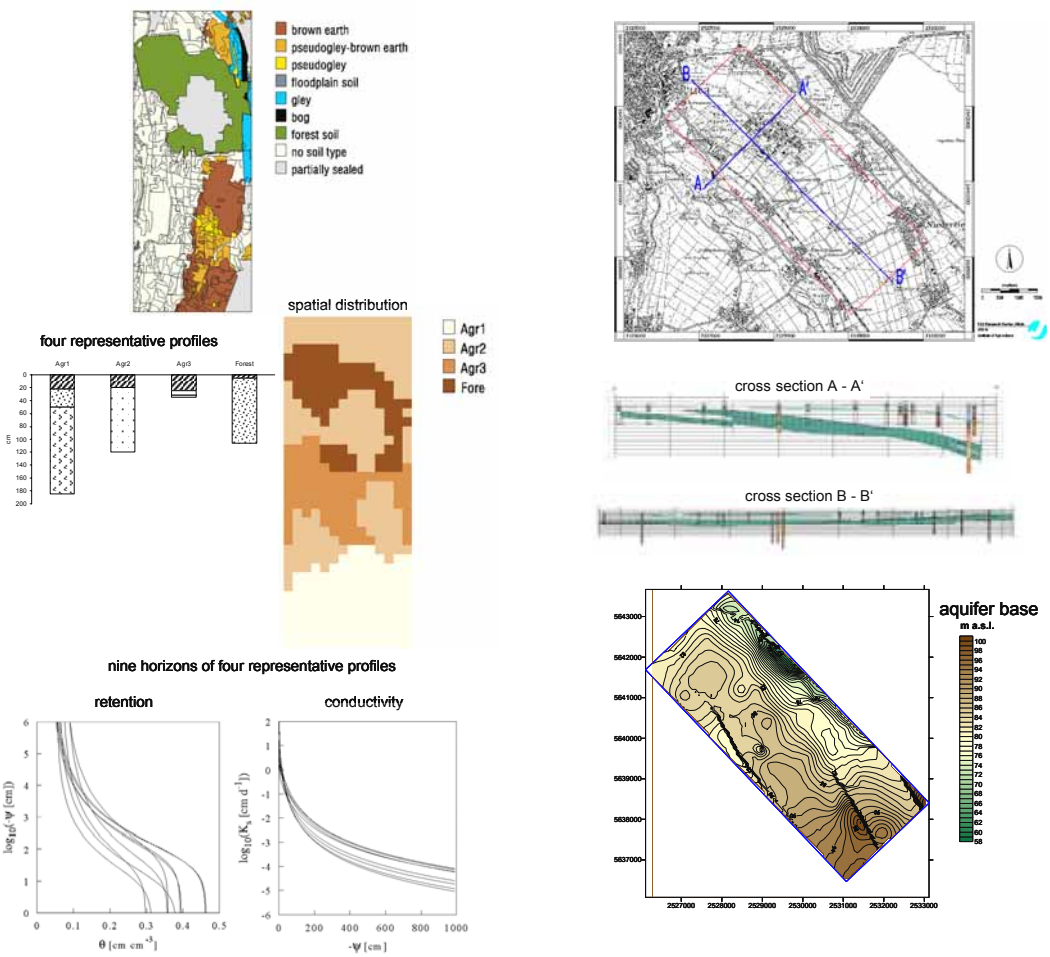

Figure 4. Original soil map (a), extracted representative soil profiles (b), water retention and hydraulic conductivity of the different soil layers estimated using a pedotransfer function (c), geological set-up along two transects, green bands are clay layers that form the aquifer basis (d), aquifer-basis depth (e)

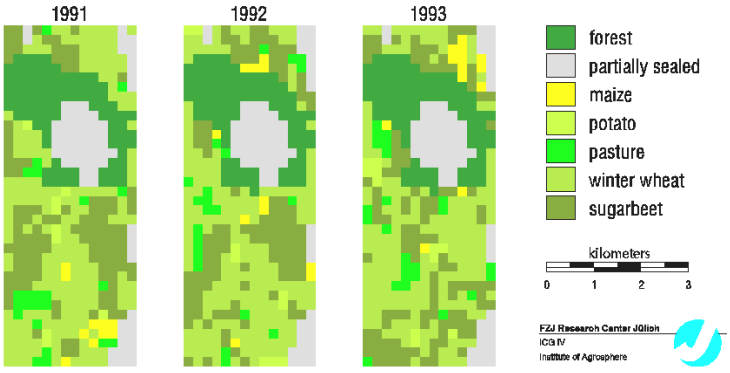

Figure 5. Land use in the PEGASE test area 'Zwischenscholle'

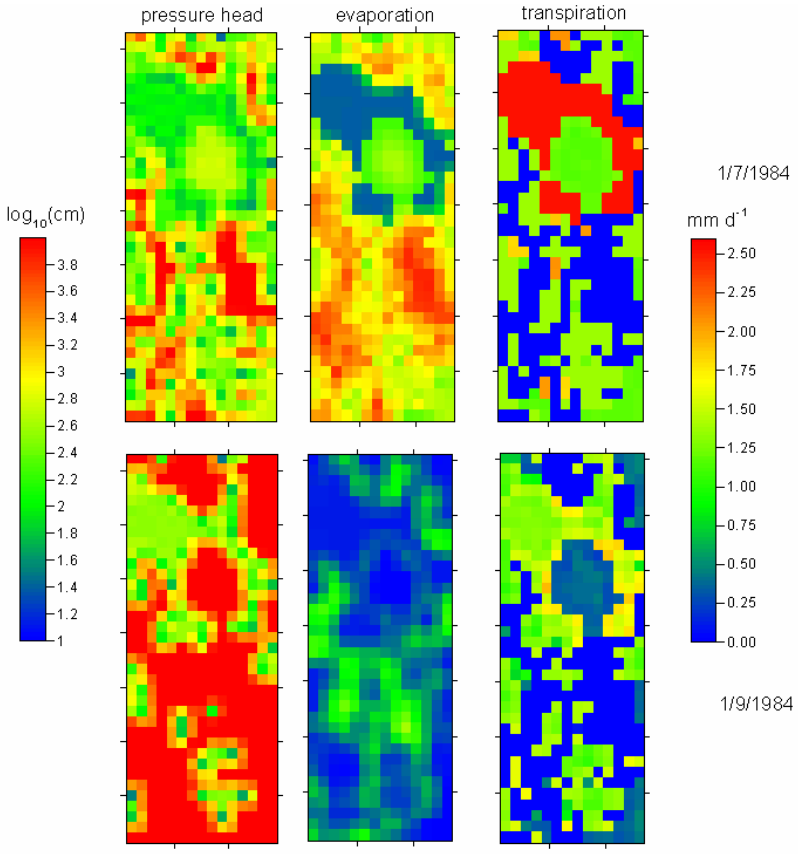

Figure 6. Simulated spatial distribution of matric potential, evaporation and transpiration rates by the TRACE model

Chapter 9.
W.G.M. Bastiaanssen, R.G. Allen, P. Droogers, G. D'Urso and P. Steduto;
Figures 1, 2 and 6

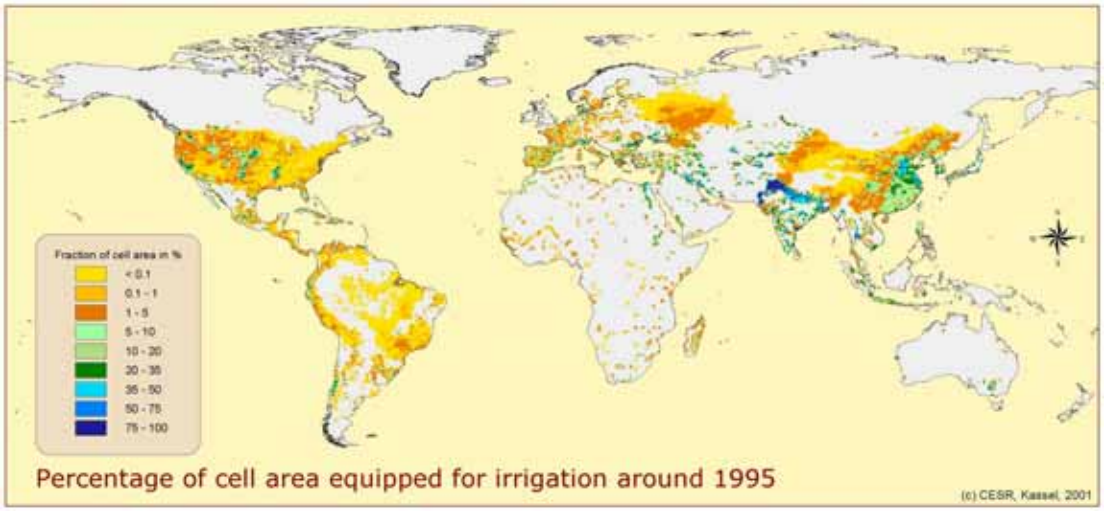

Figure 1. Fraction of area under irrigation as compiled from governmental sources and FAO (after Döll and Siebert 2000)

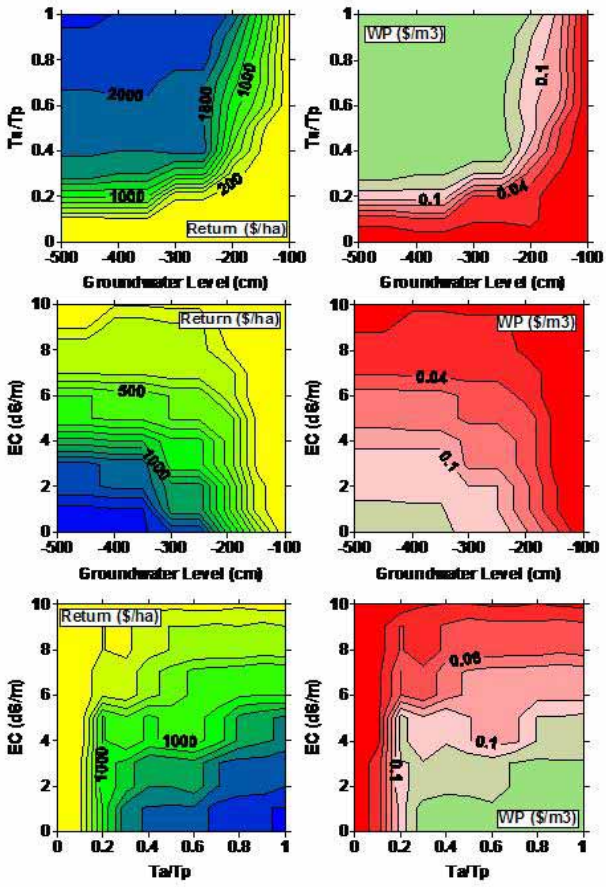

Figure 2. Caption on the next page

Figure 2 (previous page). Combined effects of groundwater level, salinity of irrigation water expressed as electric conductivity (EC) and crop water deficit expressed as relative transpiration (T_a/T_p) on the economic productivity of water (WP) in Sirsa District, India (after Droogers et al. 2003)

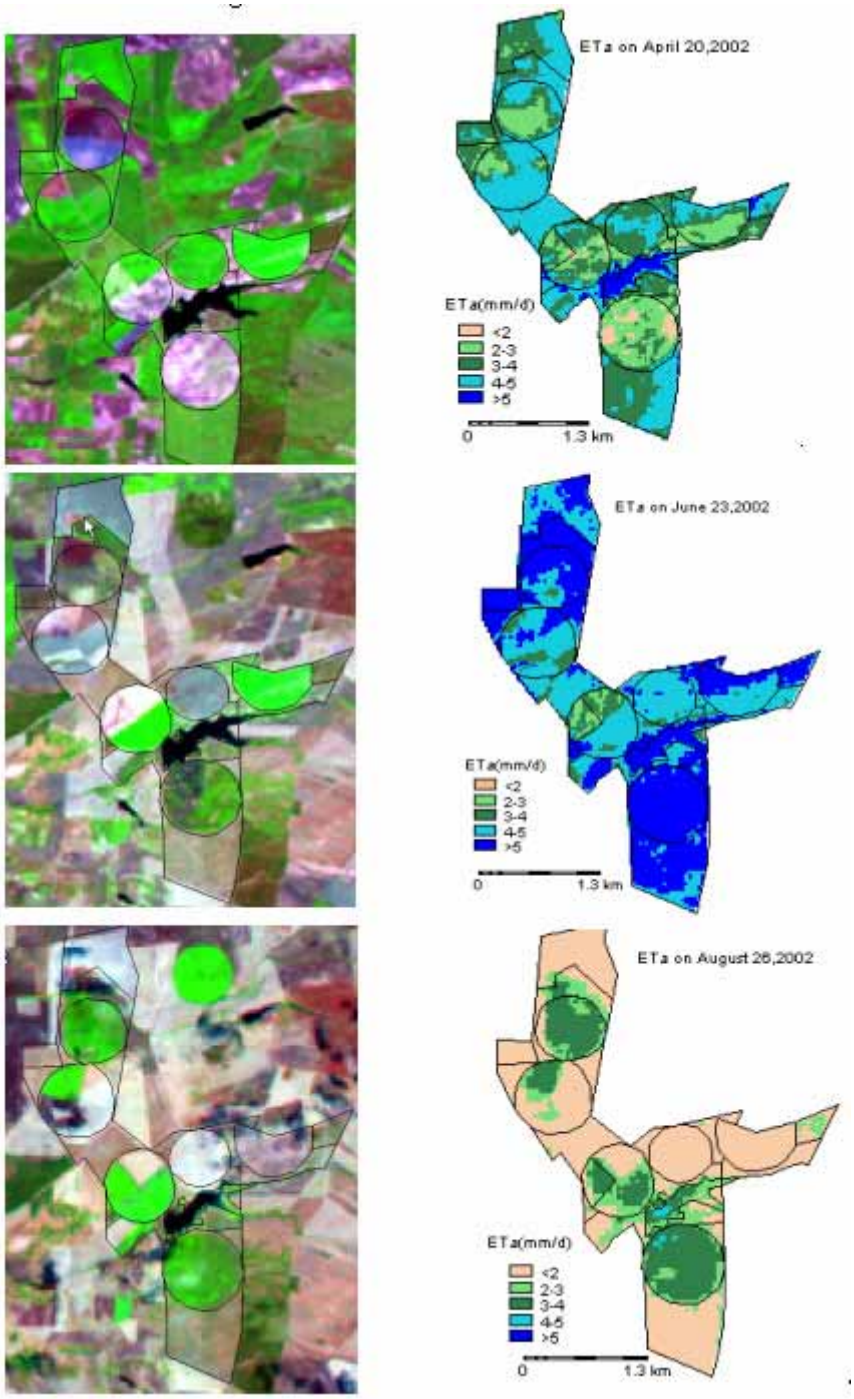

Figure 6. Progression of crop development (as false color composite on the left) and sebal-based ET (on the right) for the Serafim farm in Portugal (after Dorji 2003). It should be noted that the full processed area comprised 185 km x 185 km

Chapter 10.
J.P.M. Witte, A.F.M. Meuleman, S. van der Schaaf and B. Raterman; Figures 4, 11, 12 and 13

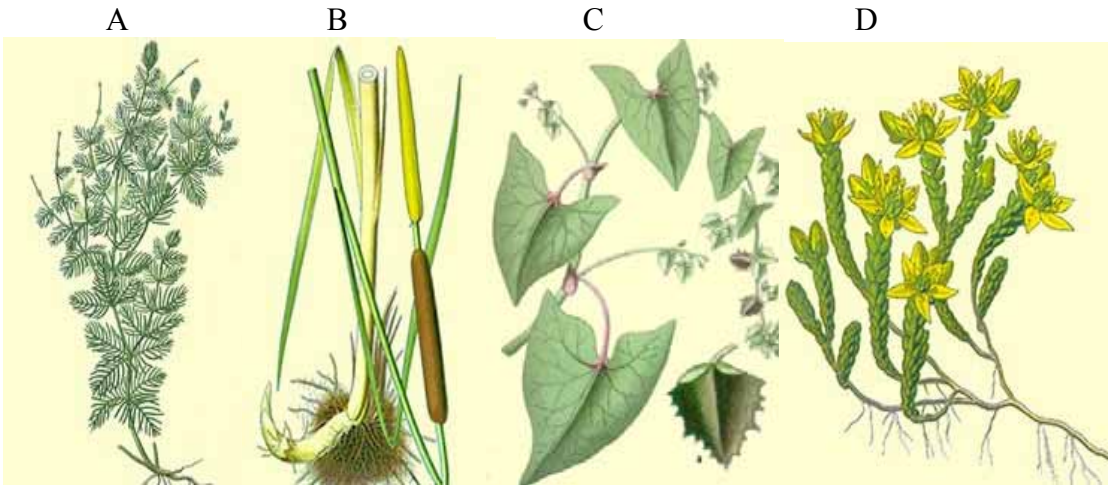

Figure 4. Examples of different categories of species, classified according to the way they are adapted to the water regime of their site: (A) a 'hydrophyte' (Alternate-flowered Water Milfoil, *Myriophyllum alterniflorum*), (B) a 'hygrophyte' (Lesser Bulrush, *Typha angustifolia*; notice its hollow stem), (C) a 'mesophyte' (Black Bindweed, *Fallopia convolvulus*) and (D) a 'xerophyte' (Biting Stonecrop, *Sedum acre*; notice its succulent morphology)

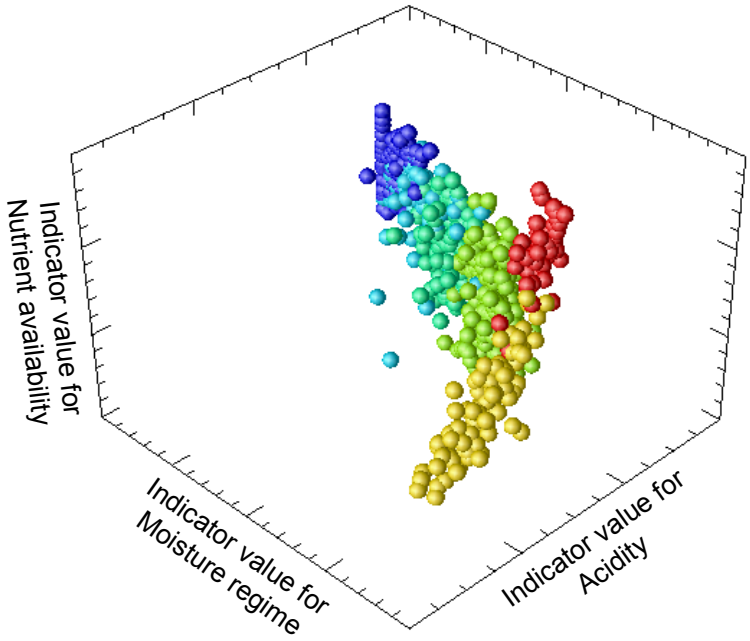

Figure 11. Classified vegetation samples (balls) plotted in relation to their average indicator values. Colors correspond to different vegetation types. Each vegetation type in this 3D-space is described by Kernel functions

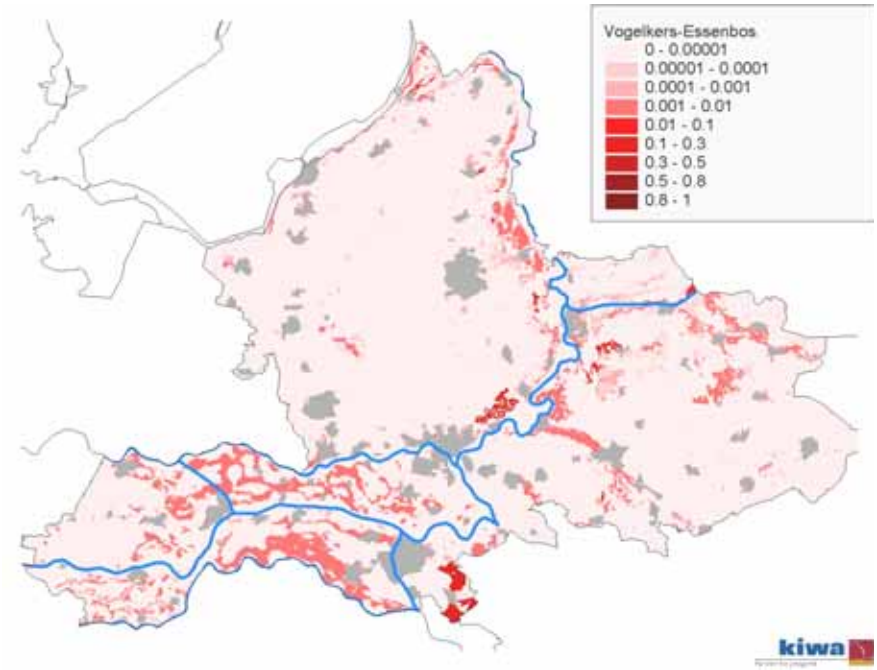

Figure 12. Occurrence probability in the province of Gelderland (The Netherlands) of the *Pruno Fraxinetum* association (defined by Stortelder et al. 1999). Since land use and atmospheric deposition of nitrogen have not been taken into account, this map shows the potential distribution

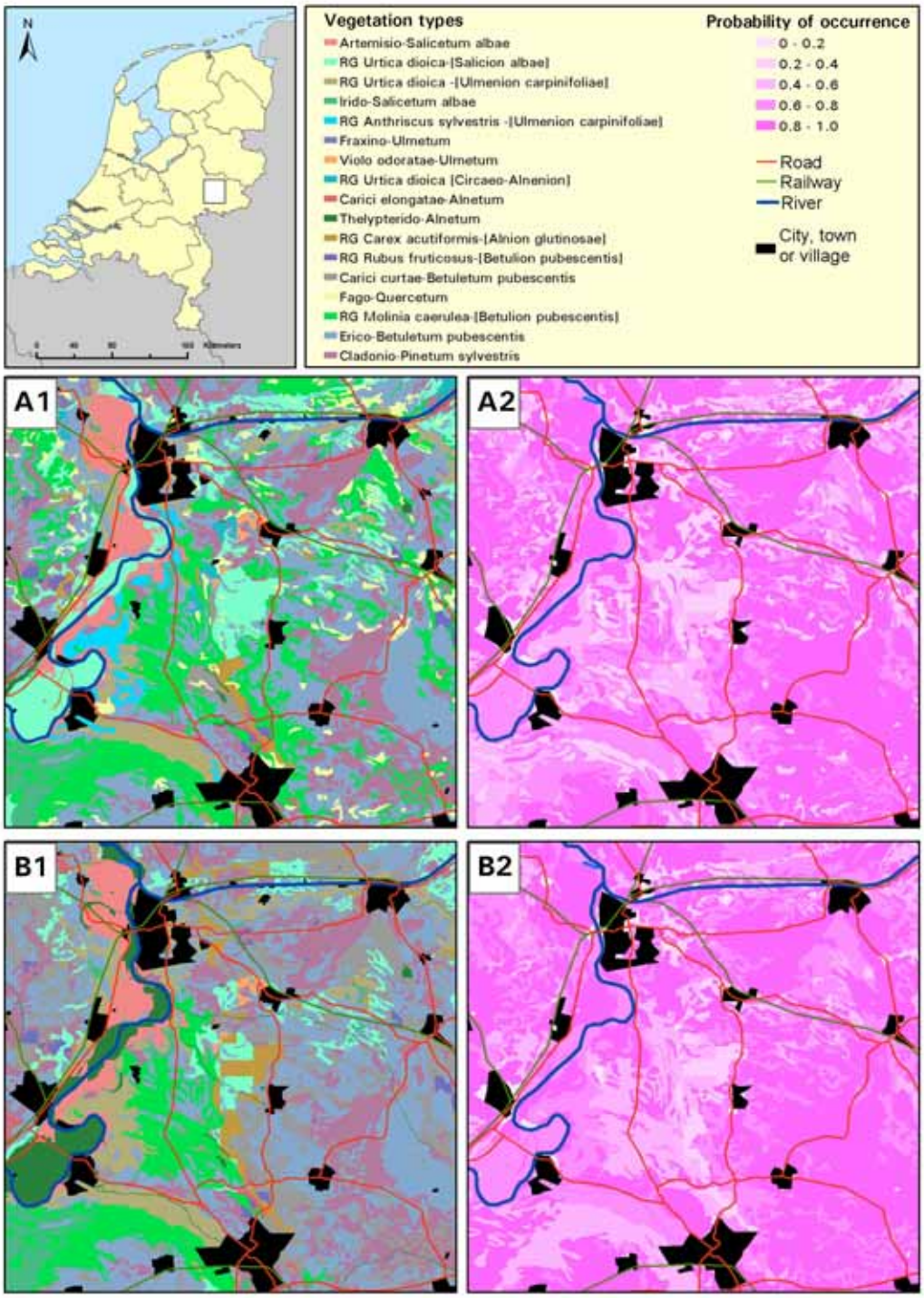

Figure 13. Vegetation maps, showing the potential distribution of vegetation types that are most likely to occur before (A1) and after (B1) a 25-cm fall of the groundwater table. Figures on the right (A2 and B2) show the occurrence probability of the predictions. Vegetation types are associations of woods according to Stortelder et al. (1999)